Multi-harmonic Rutherford island theory

Cite as: Phys. Plasmas **29**, 092501 (2022); https://doi.org/10.1063/5.0099489
Submitted: 17 May 2022 • Accepted: 13 August 2022 • Published Online: 09 September 2022

R. Fitzpatrick

Physics of Plasmas ARTICLE scitation.org/journal/php

Multi-harmonic Rutherford island theory

Cite as: Phys. Plasmas **29**, 092501 (2022); doi: 10.1063/5.0099489
Submitted: 17 May 2022 · Accepted: 13 August 2022 ·
Published Online: 9 September 2022

R. Fitzpatrick[a]

AFFILIATIONS

Department of Physics, Institute for Fusion Studies, University of Texas at Austin, Austin, Texas 78712, USA

[a]Author to whom correspondence should be addressed: rfitzp@utexas.edu

ABSTRACT

Rutherford island theory, which governs the nonlinear evolution of tearing modes in tokamak plasmas, is generalized to take into account situations in which the conventional one-harmonic approximation is not valid. The analysis incorporates non-inductive currents driven by radio frequency (RF) electromagnetic waves injected into the plasma. A multi-harmonic tearing mode dispersion relation is derived that takes the form of a nonlinear inhomogeneous matrix eigenvalue problem. The dispersion relation is solved in the so-called two-harmonic approximation, in which only the principal Fourier harmonic of the perturbed magnetic flux and its first overtone are included in the calculation. In the absence of RF current drive, the nonlinear behavior of a tearing mode predicted in the two-harmonic approximation does not differ substantially from that predicted in the one-harmonic approximation. On the other hand, RF current drive that is sufficiently localized in the vicinity of the O-points of the mode's magnetic island chain is capable of triggering bifurcations of the O-points (which is impossible in the one-harmonic approximation). However, the current drive is incapable of triggering bifurcations of the island X-points. This finding is significant because Bardóczi and Evans [Phys. Rev. Lett. **126**, 085003 (2021)] recently observed bifurcations of magnetic island chain O-points in the presence of RF current drive in the DIII-D tokamak but did not observe bifurcations of the X-points. Finally, the changes in the topology of the magnetic island flux-surfaces induced by RF current drive are found to facilitate the stabilization of the tearing mode.

I. INTRODUCTION

Tearing modes are magnetohydrodynamical (MHD) instabilities that often limit fusion plasma performance in magnetic confinement devices, such as tokamaks, which rely on nested toroidal magnetic flux-surfaces.[1,2] As the name suggests, "tearing" modes tear and reconnect magnetic field-lines, in the process converting nested toroidal flux-surfaces into helical magnetic island chains.[3] Such island chains degrade plasma confinement because heat and particles are able to travel radially from one side of the chain to the other by flowing along magnetic field-lines, which is a relatively fast process, instead of having to diffuse across magnetic flux-surfaces, which is a relatively slow process, giving rise to a flattening of the plasma pressure across the chain.[4,5]

Classical tearing modes are driven by current gradients within the plasma.[1] However, so-called *neoclassical tearing modes* (NTMs) are driven by the loss of the *bootstrap current*, which is a non-inductive current induced by plasma pressure gradients,[6] as a consequence of the flattening of the pressure gradient across the associated magnetic island chain.[7] NTMs in tokamaks are the main limitation to the achievement of an adequate level of normalized plasma pressure for the purposes of thermonuclear fusion.[8] NTMs are usually controlled in tokamaks by means of an additional non-inductive current driven in the immediate vicinity of the island chain via radio frequency (RF) electromagnetic waves injected into the plasma.[8,9] The purpose of the RF current drive is to replace the missing bootstrap current within the island chain, and, thereby, to stabilize the mode.[10] It should be noted, however, that RF current drive can also be used to stabilize classical tearing modes.[10]

The nonlinear growth of tearing modes is described by a theory that was first published almost 50 years ago by Rutherford.[3] According to Rutherford's theory:

1. Linear analysis becomes invalid as soon as the width of the magnetic island chain exceeds the linear layer width. Given that the linear layer widths in high temperature tokamak plasmas are very thin (i.e., typically a factor $S^{-2/5}$ smaller than the minor radius, where $S \gtrsim 10^8$ is the Lundquist number),[1] it follows that if a tearing mode has attained a sufficient amplitude to be detectable experimentally, then it is already in the nonlinear regime.
2. As soon as the island width exceeds the linear layer width, inertia becomes negligible in the plasma equation of motion. The absence of inertia in the equation of motion also forces the plasma current density to be constant on each magnetic flux-surface of the island chain.
3. Assuming that the tearing mode is not too unstable, the constant-ψ approximation can be employed in the immediate

vicinity of the island chain.[1] This enables a simple analytic solution for the island magnetic flux-surfaces.

4. Given that the island flux-surfaces are known and that the current density is a flux-surface function, plasma flow can be eliminated from the plasma Ohm's law, by means of a suitable flux-surface average operator, to determine the current density profile in the immediate vicinity of the island chain.
5. The current density profile in the immediate vicinity of the island chain can be used to asymptotically match the island solution to a conventional tearing mode solution, governed by linear ideal-MHD, in the remainder of the plasma to produce a tearing mode dispersion relation. According to this dispersion relation, the width of the island chain grows *linearly* in time.
6. The current density profile in the vicinity of the island chain contains multiple harmonics. In other words, if we are considering a tearing mode in a tokamak that creates an island chain with m_θ periods in the poloidal direction and n_ϕ periods in the toroidal direction, then the current density in the island region has not only a $(m_\theta,\, n_\phi)$ component but also a $(2\,m_\theta,\, 2\,n_\phi)$ component and a $(3\,m_\theta,\, 3\,n_\phi)$ component, etc. Nevertheless, the perturbed magnetic field in the island region is assumed to be dominated by the $(m_\theta,\, n_\phi)$ component. Henceforth, we shall refer to this assumption as the *one-harmonic approximation*.

A recent experimental paper by Bardóczi and Evans[11] clearly shows that the one-harmonic approximation is not necessarily valid, especially in cases in which RF-driven non-inductive currents are applied in the island region. The purpose of this paper is to examine under which circumstances the one-harmonic approximation holds good and also to devise a multi-harmonic extension to Rutherford's analysis that is capable of describing situations in which the one-harmonic approximation fails.

In this paper, for the sake of simplicity, we shall perform our analysis in slab geometry. However, the generalization to cylindrical geometry is straightforward. We shall also restrict our attention to classical tearing modes interacting with RF-driven non-inductive currents. The incorporation of the bootstrap current into the analysis is also straightforward (it is just an additional non-inductive current).

II. PRELIMINARY SLAB ANALYSIS

A. Reduced-MHD equations

Our starting point is a set of MHD equations that neglects plasma compressibility but incorporates plasma resistivity and non-inductive current drive

$$\nabla\cdot\mathbf{V}=0, \tag{1}$$

$$\rho\left[\frac{\partial\mathbf{V}}{\partial t}+(\mathbf{V}\cdot\nabla)\mathbf{V}\right]+\nabla p-\mathbf{j}\times\mathbf{B}=0, \tag{2}$$

$$\mathbf{E}+\mathbf{V}\times\mathbf{B}=\eta\,(\mathbf{j}-\mathbf{j}_{\rm ni}). \tag{3}$$

Here, $\mathbf{V}$, p, $\mathbf{j}$, $\mathbf{j}_{\rm ni}$, $\mathbf{B}$, and $\mathbf{E}$ represent the plasma flow velocity, the plasma pressure, the total plasma current density, the non-inductive component of the plasma current density, the magnetic field-strength, and the electric field-strength, respectively. Moreover, the plasma mass density, ρ, and resistivity, η, are both assumed to be spatially uniform, for the sake of simplicity. Equations (1)–(3) form a complete set when combined with the following subset of Maxwell's equations: $\nabla\cdot\mathbf{B}=0$, $\nabla\times\mathbf{E}=-\partial\mathbf{B}/\partial t$, and $\nabla\times\mathbf{B}=\mu_0\,\mathbf{j}$.

Consider a simplified slab scenario in which the Cartesian coordinate z is ignorable. In other words, there is no variation in the z-direction (i.e., $\partial/\partial z=0$). We can automatically satisfy Eq. (1) and $\nabla\cdot\mathbf{B}=0$ by writing $\mathbf{V}=\nabla\phi\times\mathbf{e}_z+V_z\,\mathbf{e}_z$ and $\mathbf{B}=\nabla\psi\times\mathbf{e}_z+B_z\,\mathbf{e}_z$, where $\mathbf{e}_z$ is a unit vector parallel to the z-axis, and V_z and B_z are the constants.

If we take the z-component of Eq. (3) and the z-component of the curl of Eq. (2), making use of Maxwell's equations, then we obtain the so-called *reduced-MHD equations*:[12]

$$\frac{\partial\psi}{\partial t}=[\phi,\psi]+\frac{\eta}{\mu_0}\,(J-J_0-J_{\rm ni}), \tag{4}$$

$$\rho\,\frac{\partial U}{\partial t}=\rho\,[\phi,U]+\mu_0^{-1}\,[J,\psi], \tag{5}$$

$$J=\nabla^2\psi, \tag{6}$$

$$U=\nabla^2\phi, \tag{7}$$

where $[A,B]\equiv\nabla A\times\nabla B\cdot\mathbf{e}_z$. Here, the plasma current density is written as $\mathbf{j}=-\mu_0^{-1}\,J\,\mathbf{e}_z$, the non-inductive current density is written as $\mathbf{j}_{\rm ni}=-\mu_0^{-1}\,J_{\rm ni}\,\mathbf{e}_z$, and $\boldsymbol{\omega}\equiv\nabla\times\mathbf{V}=-U\,\mathbf{e}_z$ is the plasma vorticity. Moreover, $J_0(x)=-(\mu_0/\eta)\,E_{z\,{\rm in}}$, where $E_{z\,{\rm in}}(x)$ is the z-directed inductive electric field that maintains the equilibrium current density.

B. Linearized reduced-MHD equations

Consider the stability of a current sheet whose equilibrium state is characterized by zero flow and

$$\mathbf{B}=B_0\,F\left(\frac{x}{a}\right)\mathbf{e}_y, \tag{8}$$

$$\mathbf{j}=\frac{B_0}{\mu_0\,a}\,F'\left(\frac{x}{a}\right)\mathbf{e}_z, \tag{9}$$

where $F(-y)=-F(y)$, $F(y)\to{\rm sgn}(y)$ as $|y|\to\infty$ and $'$ denotes the differentiation with respect to argument. Here, a is a measure of the thickness of the sheet, and B_0 is a typical value of B_y within the sheet. (Hence, in tokamak geometry, a represents the minor radius, and B_0 is the typical poloidal magnetic field-strength.) Neglecting the non-inductive current drive for the moment, we deduce from Eq. (4) that

$$J_0(x)=-\frac{B_0}{a}\,F'\left(\frac{x}{a}\right). \tag{10}$$

Suppose that the system is periodic in the y direction, with period L. (In tokamak geometry, $L=2\pi\,r_s/m_\theta$, where r_s is the minor radius of the resonant surface.) Consider a small-amplitude perturbation to the system of the form

$$\psi(x,y,t)=-B_0\int_0^x F\left(\frac{x'}{a}\right)dx'+\sum_{m=1,\infty}\psi_m(x)\,{\rm e}^{{\rm i}(mk_0y+\gamma t)}, \tag{11}$$

$$J(x,y,t)=-\frac{B_0}{a}\,F'\left(\frac{x}{a}\right)+\sum_{m=1,\infty}J_m(x)\,{\rm e}^{{\rm i}(mk_0y+\gamma t)}, \tag{12}$$

$$\phi(x,y,t)=\sum_{m=1,\infty}\phi_m(x)\,{\rm e}^{{\rm i}(mk_0y+\gamma t)}, \tag{13}$$

$$U(x,y,t)=\sum_{m=1,\infty}U_m(x)\,{\rm e}^{{\rm i}(mk_0y+\gamma t)}, \tag{14}$$

where $k_0 = 2\pi/L$. (In tokamak geometry, $k_0\, y = m_\theta\, \theta - n_\phi\, \phi$, where θ and ϕ are the poloidal and toroidal angles, respectively.)

Substituting Eqs. (11)–(14) into the reduced-MHD equations (4)–(7) and only retaining terms that are first order in small quantities, we obtain the so-called *linearized reduced-MHD equations*:

$$\gamma\, \psi_m = \mathrm{i}\, k_m\, B_0\, F\, \phi_m + \frac{\eta}{\mu_0}\left(\frac{d^2}{dx^2} - k_m^2\right)\psi_m, \tag{15}$$

$$\gamma\, \rho\left(\frac{d^2}{dx^2} - k_m^2\right)\phi_m = \mathrm{i}\, \mu_0^{-1}\, k_m\, B_0\, F\left(\frac{d^2}{dx^2} - k_m^2 - \frac{F''}{a^2\, F}\right)\psi_m, \tag{16}$$

where $k_m = m\, k_0$.

It is helpful to define the Alfvén timescale,

$$\tau_{Am} = \frac{k_m^{-1}}{(B_0^2/\mu_0\, \rho)^{1/2}}, \tag{17}$$

the resistive diffusion timescale,

$$\tau_R = \frac{\mu_0\, a^2}{\eta}, \tag{18}$$

and the Lundquist number,

$$S_m = \frac{\tau_R}{\tau_{Am}}. \tag{19}$$

It is assumed that $S_m \gg 1$.

Let $x = a\, \hat{x}$, $k_m = \hat{k}_m/a$, $\gamma = \hat{\gamma}/\tau_{Am}$, $\psi_m = -a\, B_0\, \hat{\psi}_m$, and $\phi_m = \mathrm{i}\,(\gamma\, a/k_m)\, \hat{\phi}_m$. The dimensionless normalized versions of the linearized reduced-MHD equations (15) and (16) become

$$S_m\, \hat{\gamma}\left(\hat{\psi}_m - F\, \hat{\phi}_m\right) = \left(\frac{d^2}{d\hat{x}^2} - \hat{k}_m^2\right)\hat{\psi}_m, \tag{20}$$

$$\hat{\gamma}^2\left(\frac{d^2}{d\hat{x}^2} - \hat{k}_m^2\right)\hat{\phi}_m = -F\left(\frac{d^2}{d\hat{x}^2} - \hat{k}_m^2 - \frac{F''}{F}\right)\hat{\psi}_m. \tag{21}$$

Our normalization scheme is designed such that, throughout the bulk of the plasma, $\hat{\psi}_m \sim \hat{\phi}_m$, and the only other quantities in the previous two equations whose magnitudes differ substantially from unity are $S_m\, \hat{\gamma}$ and $\hat{\gamma}^2$.

C. Asymptotic matching

Suppose that the perturbation grows on a timescale that is much less than τ_R but much greater than τ_{Am}. It follows that

$$\hat{\gamma} \ll 1 \ll S_m\, \hat{\gamma}. \tag{22}$$

Thus, throughout the bulk of the plasma, we can neglect the right-hand side of Eq. (20) and the left-hand side of Eq. (21), which is equivalent to the neglect of plasma resistivity and inertia. In this case, Eqs. (20) and (21) reduce to the so-called *linearized marginally stable ideal-MHD equations*:

$$\hat{\phi}_m = \frac{\hat{\psi}_m}{F}, \tag{23}$$

$$\frac{d^2\hat{\psi}_m}{d\hat{x}^2} - \hat{k}_m^2\, \hat{\psi}_m - \frac{F''}{F}\, \hat{\psi}_m = 0. \tag{24}$$

Equation (23) is equivalent to the well-known *flux-freezing constraint*[13] and forbids any changes in the topology of the equilibrium magnetic field-lines. However, it is clear that the linearized marginally stable ideal-MHD equations break down in the immediate vicinity of the so-called *resonant surface*, located at $x = 0$, where $F = 0$ (i.e., where B_y reverses direction). This follows from Eq. (23), which implies that $\hat{\phi}_m \to \infty$ as $F \to 0$ if $\hat{\psi}_m(0) \neq 0$ (i.e., if the topology of the magnetic field-lines changes in the vicinity of the resonant surface). [In tokamak geometry, the resonant surface is located at minor radius $r = r_s$, where $q(r_s) = m_\theta/n_\phi$. Here, $q(r) = r\, B_\phi/(R_0\, B_\theta)$ is the safety-factor profile, B_θ is the equilibrium poloidal magnetic field, and B_ϕ is the equilibrium toroidal magnetic field.[2]] In general, we need to employ the full set of reduced-MHD equations in the so-called *inner region*, close to the resonant surface, where Eqs. (23) and (24) break down. The remainder of the plasma, which is governed by the linearized marginally stable ideal-MHD equations, is known as the *outer region*.

The stability problem reduces to solving the reduced-MHD equations (4)–(7), in the inner region, solving the linearized marginally stable ideal-MHD equations (23) and (24), in the outer region, and matching the two solutions at the boundary between the inner and outer regions.[1] In general, the tearing-parity [i.e., $\hat{\psi}_m(-\hat{x}) = \hat{\psi}_m(\hat{x})$] solution of the so-called *tearing mode equation* (24), which satisfies physical boundary conditions at $|\hat{x}| \to \infty$ [i.e., $|\hat{\psi}_m| \propto \exp(-\hat{k}_m\, |\hat{x}|)$ as $|\hat{x}| \to \infty$], has a gradient discontinuity across the resonant surface.[1] Note that the adopted boundary conditions assume that the plasma is isolated. In other words, the plasma is not subject to any externally generated magnetic perturbations. It is helpful to define the *tearing stability index*,[1]

$$\Delta'_m = \left[\frac{1}{\hat{\psi}_m}\frac{d\hat{\psi}_m}{d\hat{x}}\right]_{\hat{x}=0_-}^{\hat{x}=0_+}. \tag{25}$$

This real dimensionless quantity is uniquely determined by the tearing mode equation and the boundary conditions, for each mode number, m.

Let $W_1 \ll a$ be the thickness (in x) of the inner region. Our task is, thus, to solve the reduced-MHD equations (4)–(7), in the inner region, subject to the matching condition [see Eqs. (11) and (25)]

$$\psi(\hat{x}, \xi, t) \to -B_0\, a\, F'(0)\, \frac{\hat{x}^2}{2} + \sum_{m=1,\infty} \Psi_m(t)\left(1 + \frac{1}{2}\, \Delta'_m\, |\hat{x}|\right)\cos(m\, \xi - \varphi_m), \tag{26}$$

as $|x|/W_1 \to \infty$. Here, $\xi = k_0\, y$, and the Ψ_m and φ_m are the real. Note that the system is periodic in ξ, with period 2π. (In tokamak geometry, $\xi = m_\theta\, \theta - n_\varphi\, \phi$.)

III. MULTI-HARMONIC CLASSICAL RUTHERFORD ISLAND THEORY

A. Introduction

In this section, we shall develop the theory of a multi-harmonic classical tearing mode interacting with non-inductive RF current drive.

B. Normalization scheme

Let $t = \tau_R\, \hat{t}$, $\psi = -B_0\, a\, F'(0)\, \hat{\psi}$, $\Psi_m = -B_0\, a\, F'(0)\, \hat{\Psi}_m$, $J = -(B_0/a)\, F'(0)(1 + \hat{J})$, $J_{\rm ni} = -(B_0/a)\, F'(0)\, \hat{J}_{\rm ni}$, $\phi = (a/k_0\, \tau_R)\, \hat{\phi}$, and $U = (1/a\, k_0\, \tau_R)\, \hat{U}$. The reduced-MHD equations (4)–(7) yield

$$\frac{\partial \hat{\psi}}{\partial \hat{t}} = \{\hat{\phi}, \hat{\psi}\} + \hat{J} - \hat{J}_{\rm ni}, \tag{27}$$

$$\frac{\partial \hat{U}}{\partial \hat{t}} = \{\hat{\phi}, \hat{U}\} + S^2 \{\hat{J}, \hat{\psi}\}, \tag{28}$$

$$\frac{\partial^2 \hat{\psi}}{\partial \hat{x}^2} = 1 + \hat{J}, \tag{29}$$

$$\hat{U} = \frac{\partial^2 \hat{\phi}}{\partial \hat{x}^2}, \tag{30}$$

in the inner region, where

$$\{A, B\} \equiv \frac{\partial A}{\partial \hat{x}} \frac{\partial B}{\partial \xi} - \frac{\partial A}{\partial \xi} \frac{\partial B}{\partial \hat{x}}, \tag{31}$$

$$S = \frac{\tau_R}{\tau_H}, \tag{32}$$

$$\tau_H = \frac{1}{k_0 F'(0)} \left(\frac{\mu_0 \rho}{B_0^2}\right)^{1/2}, \tag{33}$$

and we have assumed that $k_m W_1 \ll 1$. Note that we have included the non-inductive RF current drive in Eq. (27), while neglecting it in the outer region, because we are assuming that the current drive is only applied in the inner region. As before, the modified Lundquist number, S, is assumed to be much greater than unity. Moreover, the matching condition (26) gives

$$\hat{\psi}(\hat{x}, \xi, \hat{t}) \rightarrow \frac{\hat{x}^2}{2} + \sum_{m=1,\infty} \hat{\Psi}_m(\hat{t}) \left(1 + \frac{\Delta'_m}{2} |\hat{x}|\right) \cos(m\xi - \varphi_m), \tag{34}$$

as $|\hat{x}|/\hat{W}_1 \rightarrow \infty$, where $W_1 = a\, \hat{W}_1$.

C. Ordering scheme

Now, we are assuming that $\hat{W}_1 \ll 1$. In other words, we are assuming that the thickness of the inner region is much less than that of the equilibrium current sheet. In the inner region, $\hat{t} \sim \hat{W}_1$ (as will become apparent), $\hat{x} \sim \hat{W}_1$, $\xi \sim 1$, $\hat{\psi} \sim \hat{W}_1^2$, $\hat{J} \sim \hat{W}_1$ (this is consistent with $\Delta'_m \sim 1$), $\hat{J}_{\rm ni} \sim \hat{W}_1$ (by assumption), $\hat{\phi} \sim 1$, and $\hat{U} \sim 1/\hat{W}_1^2$. It follows that all terms in Eqs. (27) and (30) are of the same order of magnitude. On the other hand, the terms involving $\hat{U}$ in Eq. (28) are smaller than the other term by a factor $(\hat{\delta}/\hat{W}_1)^5$, where $\hat{\delta} = S^{-2/5}$ is the (normalized) linear layer width.[1] Finally, the term involving $\hat{J}$ in Eq. (29) is smaller than the other terms by a factor $\hat{W}_1$. Thus, assuming that $\hat{\delta} \ll \hat{W}_1 \ll 1$ (i.e., the inner region is much wider than the linear layer width but much thinner than the equilibrium current sheet width), Eqs. (27)–(30) reduce to

$$\frac{\partial \hat{\psi}}{\partial \hat{t}} = \{\hat{\phi}, \hat{\psi}\} + \hat{J} - \hat{J}_{\rm ni}, \tag{35}$$

$$\{\hat{J}, \hat{\psi}\} = 0, \tag{36}$$

$$\frac{\partial^2 \hat{\psi}}{\partial \hat{x}^2} = 1. \tag{37}$$

Note that plasma inertia has dropped out of Eq. (36).

D. Analysis

Equation (37) can be integrated, subject to the matching condition (34) to give

$$\hat{\psi}(\hat{x}, \xi, \hat{t}) = \frac{\hat{x}^2}{2} + \sum_{m=1,\infty} \hat{\Psi}_m(\hat{t}) \cos(m\xi - \varphi_m), \tag{38}$$

in the inner region. The previous equation is consistent with Eq. (34) provided that $|\Delta'_m|\, \hat{W}_1 \ll 1$, for all m. This ordering is known as the *constant-ψ approximation*[1] and is automatically satisfied if $|\Delta'_m| \sim 1$ and $\hat{W}_1 \ll 1$.

Equation (36) implies that

$$\hat{J} = \hat{J}(\hat{\psi}). \tag{39}$$

In other words, the current density in the island region is a flux-surface function (i.e., it is constant on magnetic field lines). We shall also assume that

$$\hat{J}_{\rm ni} = \hat{J}_{\rm ni}(\hat{\psi}) \tag{40}$$

because non-inductive RF current drive is due to the action of fast electrons that very rapidly equilibrate on magnetic flux surfaces.

Equation (35) can be combined with the previous three equations to give

$$\sum_{m=1,\infty} \frac{d\hat{\Psi}_m}{d\hat{t}} \cos(m\xi - \varphi_m) = \{\hat{\phi}, \hat{\psi}\} + \hat{J}(\hat{\psi}) - \hat{J}_{\rm ni}(\hat{\psi}). \tag{41}$$

Suppose that

$$\frac{d\hat{\Psi}_m}{d\hat{t}} = \tilde{\gamma}\, \hat{\Psi}_m \tag{42}$$

for all m. This assumption is reasonable if the $m = 1$ mode is the only intrinsically unstable mode, and the $m > 1$ modes are driven via nonlinear coupling to the $m = 1$ mode (see Sec. III G). Let us suppose that this is the case. [Note that the previous equation is not equivalent to assuming that the $\hat{\Psi}_m$ vary exponentially in time because $\tilde{\gamma}$ is proportional to the inverse of the island width, see Eq. (48).] Furthermore, let us write

$$\hat{W}_1 = 4\, \hat{\Psi}_1^{1/2}, \tag{43}$$

$$X = \frac{4\,\hat{x}}{\hat{W}_1}, \tag{44}$$

$$\hat{\psi}(\hat{x}, \xi, \hat{t}) = \hat{\Psi}_1(\hat{t})\, \Omega(X, \xi), \tag{45}$$

$$\epsilon_m = \frac{\hat{\Psi}_m}{\hat{\Psi}_1}. \tag{46}$$

Thus, $W_1 = \hat{W}_1\, a$ is the full width of the magnetic separatrix of the island chain that would develop in the inner region if $\epsilon_m = 0$ for $m > 1$ (i.e., if the one-harmonic approximation were valid) (see Sec. IV). Note that the ϵ_m is independent of time.

Equations (42) and (43) imply that

$$\frac{d\hat{W}_1}{d\hat{t}} = \lambda, \tag{47}$$

where

$$\lambda = \frac{\tilde{\gamma}\, \hat{W}_1}{2}. \tag{48}$$

Note that $\lambda \sim 1$, according to our ordering assumptions. Furthermore, λ is independent of time. Equations (38) and (43)–(46) yield

$$\Omega(X,\xi) = \frac{X^2}{2} + f(\xi), \tag{49}$$

where

$$f(\xi) = \sum_{m=1,\infty} \epsilon_m \cos(m\,\xi - \varphi_m). \tag{50}$$

Finally, Eq. (41) reduces to

$$\frac{\lambda\,\hat{W}_1}{8} f(\xi) = \{\hat{\phi},\hat{\psi}\} + \hat{J}(\hat{\psi}) - \hat{J}_{\rm ni}(\hat{\psi}). \tag{51}$$

E. Flux-surface average operator

According to Eq. (49),

$$X = s\sqrt{2[\Omega - f(\xi)]}, \tag{52}$$

where $s \equiv \mathrm{sgn}(X)$. Now,

$$\{\hat{\phi},\hat{\psi}\} = -\hat{x}\frac{\partial\hat{\phi}}{\partial\xi}\bigg|_\Omega = -\frac{\hat{W}_1}{4}\,s\sqrt{2[\Omega - f(\xi)]}\,\frac{\partial\hat{\phi}}{\partial\xi}\bigg|_\Omega. \tag{53}$$

The *flux-surface average operator*[3] is defined

$$\langle A(\Omega,\xi)\rangle = \int_0^{2\pi} \frac{A(\Omega,\xi)\,H(\Omega,\xi)}{\sqrt{2[\Omega - f(\xi)]}}\,\frac{d\xi}{2\pi}, \tag{54}$$

where

$$H(\Omega,\xi) = \begin{cases} 1 & \Omega \geq f(\xi) \\ 0 & \Omega < f(\xi) \end{cases}. \tag{55}$$

It follows that

$$\langle\{\hat{\phi},\hat{\psi}\}\rangle = 0, \tag{56}$$

because $\hat{\phi}(\hat{x},\xi,\hat{t})$ is periodic in ξ, with period 2π, and $\hat{\phi}(\hat{x},\xi,\hat{t})$ is odd in $\hat{x}$ [so $\hat{\phi}(0,\xi,\hat{t}) = 0$]. Thus, the flux-surface average of Eq. (51) yields

$$\hat{J}(\Omega) = \frac{\lambda\,\hat{W}_1}{8}\,\frac{\langle f(\xi)\rangle}{\langle 1\rangle} + \hat{J}_{\rm ni}(\Omega). \tag{57}$$

F. Asymptotic matching

According to the matching condition (34),

$$2\int_{-\infty}^{\infty}\int_0^{2\pi} \frac{\partial^2\hat{\psi}}{\partial\hat{x}^2}\cos(m\,\xi - \varphi_m)\,d\hat{x}\,\frac{d\xi}{2\pi} = \Delta'_m\,\hat{\Psi}_m, \tag{58}$$

$$2\int_{-\infty}^{\infty}\int_0^{2\pi} \frac{\partial^2\hat{\psi}}{\partial\hat{x}^2}\sin(m\,\xi - \varphi_m)\,d\hat{x}\,\frac{d\xi}{2\pi} = 0, \tag{59}$$

for $m = 1,\infty$. Equation (59) follows because the Δ'_m are all real quantities. The previous two equations can be combined with Eq. (29) to give

$$2\int_{-\infty}^{\infty}\int_0^{2\pi} \hat{J}(\Omega)\cos(m\,\xi - \varphi_m)\,d\hat{x}\,\frac{d\xi}{2\pi} = \Delta'_m\,\hat{\Psi}_m, \tag{60}$$

$$2\int_{-\infty}^{\infty}\int_0^{2\pi} \hat{J}(\Omega)\sin(m\,\xi - \varphi_m)\,d\hat{x}\,\frac{d\xi}{2\pi} = 0. \tag{61}$$

It is easily demonstrated that

$$d\hat{x}\,d\xi = \frac{(\hat{W}_1/4)\,d\Omega\,d\xi}{s\sqrt{2[\Omega - f(\xi)]}}. \tag{62}$$

Hence, making use of Eq. (54), Eqs. (60) and (61) reduce to

$$\hat{W}_1\int_{\Omega_{\rm min}}^{\infty} \hat{J}(\Omega)\,\langle\cos(m\,\xi - \varphi_m)\rangle\,d\Omega = \Delta'_m\,\hat{\Psi}_m, \tag{63}$$

$$\hat{W}_1\int_{\Omega_{\rm min}}^{\infty} \hat{J}(\Omega)\,\langle\sin(m\,\xi - \varphi_m)\rangle\,d\Omega = 0. \tag{64}$$

Here, $\Omega_{\rm min}$ is equal to the minimum value of $f(\xi)$.

The only obvious way of satisfying the constraints (64) is to set all of the phase angles, φ_m, equal to one another. In fact, without loss of generality, we can set all of the phase angles equal to zero. In this case,

$$f(\xi) = \sum_{m=1,\infty} \epsilon_m \cos(m\,\xi), \tag{65}$$

and Eqs. (63) and (64) become

$$\hat{W}_1\int_{\Omega_{\rm min}}^{\infty} \hat{J}(\Omega)\,\langle\cos(m\,\xi)\rangle\,d\Omega = \Delta'_m\,\hat{\Psi}_m, \tag{66}$$

$$\hat{W}_1\int_{\Omega_{\rm min}}^{\infty} \hat{J}(\Omega)\,\langle\sin(m\,\xi)\rangle\,d\Omega = 0. \tag{67}$$

Equation (67) is now automatically satisfied because $\hat{J}(\Omega)$ is an even function of ξ [since $\Omega = X^2/2 + f(\xi)$ is an even function of ξ].

Let us adopt a simplified current drive model in which

$$\hat{J}_{\rm ni}(\Omega) = \begin{cases} -\mu\,\hat{W}_1 & \Omega_{\rm min} \leq \Omega \leq \Omega_c \\ 0 & \Omega > \Omega_c, \end{cases} \tag{68}$$

where μ is a constant. Thus, the non-inductive current density takes a uniform value within (i.e., closer to the resonant surface) the magnetic flux-surface $\Omega = \Omega_c$ and is zero, otherwise.

Equations (43), (57), (65), (66), and (68) yield the tearing mode dispersion relation

$$\Delta'_m\,\epsilon_m = \lambda\sum_{m'=1,\infty} I_{m,m'}\,\epsilon_{m'} + \mu\,K_m, \tag{69}$$

where

$$I_{m,m'} = 2\int_{\Omega_{\rm min}}^{\infty} \frac{C_m(\Omega)\,C_{m'}(\Omega)}{C_0(\Omega)}\,d\Omega, \tag{70}$$

$$K_m = -16\int_{\Omega_{\rm min}}^{\Omega_c} C_m(\Omega)\,d\Omega, \tag{71}$$

$$C_m(\Omega) = \langle\cos(m\,\xi)\rangle. \tag{72}$$

The tearing mode dispersion relation, (69), takes the form of a nonlinear inhomogeneous matrix eigenvalue problem. The problem is nonlinear because the matrix elements are functions of the components of the normalized eigenvector. In general, the tearing mode dispersion relation is difficult to solve because of the great multiplicity of possible magnetic flux-surface topologies in the island region.

Note that $I_{m,m'} \sim 1$ and $K_m \sim 1$. Thus, assuming that $\Delta'_m \sim 1$ and $\mu \sim 1$, it follows from Eq. (69) that $\lambda \sim 1$, which justifies our previous assumption that $\hat{t} \sim \hat{W}_1$. Incidentally, the ordering $\mu \sim 1$

implies that the RF-driven non-inductive current density in the inner region is smaller than the equilibrium current density by a factor $\hat{W}_1$ [see Eq. (68)]. Nevertheless, according to Eq. (69), this level of RF current drive is still able to affect the growth of the tearing mode. This finding is significant because it would be completely impractical to generate a non-inductive RF current density in the inner region that competes with the equilibrium current density. Note, finally, that if $\lambda \sim 1$ then the tearing mode grows on the timescale $\hat{W}_1\,\tau_R$, which is much less than τ_R but much greater than τ_{Am}, as was previously assumed.

G. Discussion

As can easily be demonstrated, the general time evolution of the various Fourier harmonics of the perturbed magnetic flux at the resonant surface

$$\hat{\psi}(0,\xi,\hat{t}) = \sum_{m=1,\infty} \hat{\Psi}_m(\hat{t})\,\cos(m\,\xi), \tag{73}$$

is governed by the following set of coupled nonlinear ordinary differential equations:

$$\frac{\hat{W}_1}{2}\sum_{m'=1,\infty} I_{m,m'}\,\frac{d\hat{\Psi}_{m'}}{d\hat{t}} = \Delta'_m\,\hat{\Psi}_m - \mu\,K_m\,\hat{\Psi}_1. \tag{74}$$

Equation (69) describes a particular solution of this set of equations which is such that

$$\hat{W}_1(\hat{t}) = \hat{W}_1(0) + \lambda\,\hat{t}, \tag{75}$$

$$\hat{\Psi}_m(\hat{t}) = \epsilon_m\,\hat{\Psi}_1(0)\left[1+\frac{\lambda\,\hat{t}}{\hat{W}_1(0)}\right]^2. \tag{76}$$

In fact, substitution of Eq. (76) into Eq. (74) leads directly to Eq. (69), with the aid of Eq. (46). The attraction of the particular solution (76) is that the $\hat{\Psi}_m/\hat{\Psi}_1 = \epsilon_m$ ratios are independent of time. This is important because the $I_{m,m'}$ and K_m integrals depend on these ratios. A general solution of the governing differential equations, (74), is characterized by time-varying $\hat{\Psi}_m/\hat{\Psi}_1$ ratios. In this case, the $I_{m,m'}$ and K_m integrals would have to be recalculated at every time step. Under these circumstances, Rutherford theory loses its appeal, because it would be simpler to attempt a direct numerical solution of the reduced-MHD equations. (Note that this argument does not hold in the conventional single-harmonic approximation where there is only one ratio, $\hat{\Psi}_1/\hat{\Psi}_1 = 1$, whose value remains constant, irrespective of how $\hat{\Psi}_1(\hat{t})$ varies with time. However, in general, the same does not hold true in the multi-harmonic case.) Although we have chosen the particular solution (76) for mathematical convenience, the solution makes physical sense, because if there is only one unstable linear tearing mode harmonic (i.e., the $m=1$ harmonic), then we would expect this harmonic to evolve into a coherent nonlinear mode with a non-mutable harmonic structure.

IV. ONE-HARMONIC APPROXIMATION

A. Analysis

Suppose that $\epsilon_1 = 1$ and $\epsilon_m = 0$ for $m > 1$, which is the essence of the one-harmonic approximation. In this case,

$$f(\xi) = \cos\xi, \tag{77}$$

$$\Omega(X,\xi) = \frac{X^2}{2} + \cos\xi. \tag{78}$$

Note that, for $0 \le \xi < 2\pi$, $f(\xi)$ attains its maximum value, 1, at $\xi = 0$, and its minimum value, –1, at $\xi = \pi$. Figure 1 shows the contours of the normalized magnetic flux, $\Omega(X,\xi)$, in the one-harmonic approximation. It can be seen that the tearing mode has changed the topology of the magnetic field in the immediate vicinity of the resonant surface, by breaking and reconnecting magnetic field-lines, to produce a chain of magnetic islands. The magnetic separatrix, which separates the reconnected magnetic field-lines from the unreconnected field-lines, corresponds to the contour $\Omega = 1$. There is a chain of magnetic X-points located at $\xi = n\,2\pi$, where n is an integer, which are all connected by the separatrix. Such X-points are termed *heteroclinic*. Moreover, there are magnetic O-points, located at $\xi = (2n-1)\,\pi$, in the regions enclosed by the separatrix. The full width of the separatrix in X is 4, which corresponds to a full width of $\hat{W}_1$ in $\hat{x}$ [see Eq. (44)].

According to Eqs. (54), (55), (72), and (77),

$$C_m(\Omega) = \int_0^{2\pi} \frac{\cos(m\,\xi)\,H(\Omega,\xi)}{\sqrt{2(\Omega-\cos\xi)}}\,\frac{d\xi}{2\pi}, \tag{79}$$

where

$$H(\Omega,\xi) = \begin{cases} 1 & \Omega \ge \cos\xi \\ 0 & \Omega < \cos\xi. \end{cases} \tag{80}$$

Hence, we deduce that

$$C_m(\Omega \ge 1) = \int_0^{2\pi} \frac{\cos(m\,\xi)}{\sqrt{2(\Omega-\cos\xi)}}\,\frac{d\xi}{2\pi} \tag{81}$$

and

$$C_m(-1 \le \Omega < 1) = \int_{\xi_0}^{2\pi-\xi_0} \frac{\cos(m\,\xi)}{\sqrt{2(\Omega-\cos\xi)}}\,\frac{d\xi}{2\pi}, \tag{82}$$

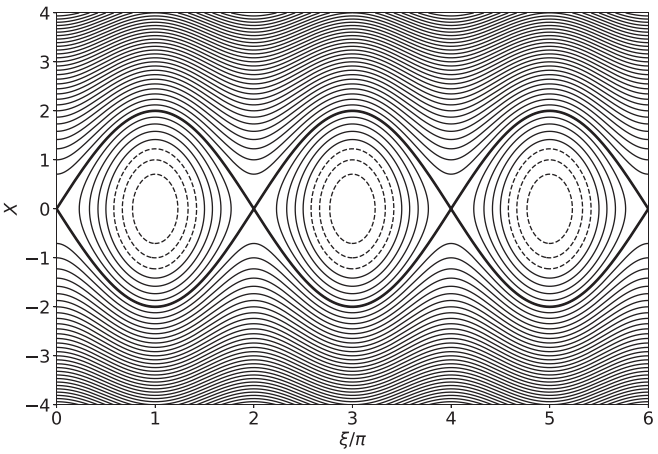

FIG. 1. Contours of the normalized magnetic flux, $\Omega(X,\xi)$, in the one-harmonic approximation. Positive/negative contours are shown as solid/dashed lines. The magnetic separatrix is shown as a bold line.

where $\xi_0 = \cos^{-1}(\Omega)$. Here, $0 \leq \xi_0 \leq \pi$.

It is helpful to define $p = \sqrt{(\Omega+1)/2}$. Thus, $p = 0$ at the magnetic O-points, and $p = 1$ at the magnetic X-points and on the magnetic separatrix. In the region $p \geq 1$, which lies outside the magnetic separatrix, let $\sin\varphi = \cos(\xi/2)$. It follows that

$$C_m(p \geq 1) = \frac{1}{\pi}\int_0^{\pi/2} \frac{\cos\left[2\,m\,\cos^{-1}(\sin\varphi)\right]}{\sqrt{p^2 - \sin^2\varphi}}\,d\varphi. \tag{83}$$

In the region $0 \leq p < 1$, which lies inside the magnetic separatrix, let $\sin\varphi = \cos(\xi/2)/\cos(\xi_0/2) = \cos(\xi/2)/p$. It follows that

$$C_m(0 \leq p < 1) = \frac{1}{\pi}\int_0^{\pi/2} \frac{\cos\left[2\,m\,\cos^{-1}(p\,\sin\varphi)\right]}{\sqrt{1 - p^2\,\sin^2\varphi}}\,d\varphi. \tag{84}$$

The tearing mode dispersion relation (69) yields

$$\Delta_1' = \lambda\, I_{1,1} + \mu\, K_1(p_c), \tag{85}$$

where

$$I_{m,m'} = 8\int_0^\infty \frac{p\,C_m(p)\,C_{m'}(p)}{C_0(p)}\,dp, \tag{86}$$

$$K_m = -64\int_0^{p_c} p\,C_m(p)\,dp, \tag{87}$$

and $p_c = \sqrt{(\Omega_c+1)/2}$.

B. Results

Equation (85) can be rearranged to give

$$\lambda = \frac{\Delta_1' - \mu\,K_1(p_c)}{I_{1,1}}. \tag{88}$$

Now, $I_{1,1}$ takes the value 0.8227,[3] whereas the function $K_1(p_c)$ is shown in Fig. 2. We can see that, in the absence of RF current drive (i.e., when $\mu = 0$), if the $m = 1$ mode is intrinsically unstable (i.e., if $\Delta_1' > 0$), then the island width grows linearly in time [see Eq. (47)] at the rate $\Delta_1'/I_{1,1}$.[3] Moreover, the application of RF current drive causes the growth rate to decrease linearly with increasing normalized RF-driven non-inductive current density, μ. The tearing mode is stabilized when μ exceeds the critical value

$$\mu_{\rm crit} = \frac{\Delta_1'}{K_1(p_c)}. \tag{89}$$

As is clear from Fig. 2, the critical RF current density required to stabilize the mode is minimized when $p_c \sim 1$. In other words, when the region in which the RF current is driven corresponds to the region lying between the magnetic O-points and the magnetic separatrix.

Note that Eq. (88) can be rewritten in the form

$$I_{1,1}\,\frac{d\hat{W}_1}{d\hat{t}} = \Delta_1' + \frac{16}{\hat{W}_1}\int_{-1}^{\infty} \hat{J}_{\rm ni}(\Omega)\,\langle\cos\xi\rangle\,d\Omega, \tag{90}$$

where Eqs. (47), (68), (71), and (72) are used. The previous equation is equivalent to similar equations derived in Refs. 14 and 15.

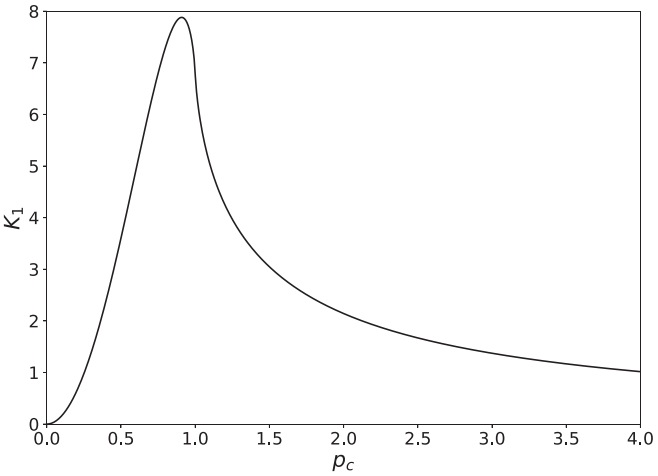

FIG. 2. The current-drive function, $K_1(p_c)$, evaluated in the one-harmonic approximation.

V. TWO-HARMONIC APPROXIMATION

A. Analysis

1. Introduction

Suppose that $\epsilon_1 = 1$, $\epsilon_2 \neq 0$, and $\epsilon_m = 0$ for $m > 2$. In other words, suppose that the $m = 2$ harmonic is included in the calculation, but the $m > 2$ harmonics are neglected. This scheme is known as the *two-harmonic approximation*. It follows that

$$f(\xi) = \cos\xi + \epsilon_2\,\cos(2\xi), \tag{91}$$

$$\Omega(X,\xi) = \frac{X^2}{2} + \cos\xi + \epsilon_2\,\cos(2\,\xi). \tag{92}$$

2. $-1/4<\epsilon_2<1/4$

Suppose that $-1/4 < \epsilon_2 < 1/4$. In this case, for $0 \leq \xi < 2\pi$, $f(\xi)$ attains its maximum value, $1+\epsilon_2$, at $\xi = 0$, and its minimum value, $-1+\epsilon_2$, at $\xi = \pi$. The topology of the magnetic field in the vicinity of the resonant surface is shown in Fig. 1. It can be seen that there is series of heteroclinic magnetic X-points connected by a magnetic separatrix that extends over all values of ξ and encloses a chain of magnetic islands each containing a single magnetic O-point.

We can write

$$C_m(\Omega)(\Omega \geq 1+\epsilon_2) = \int_0^{2\pi} \frac{\cos(m\,\xi)}{\sqrt{2[\Omega - \cos\xi - \epsilon_2\,\cos(2\,\xi)]}}\,\frac{d\xi}{2\pi} \tag{93}$$

and

$$C_m(\Omega)(-1+\epsilon_2 \leq \Omega < 1+\epsilon_2) = \int_{\xi_0}^{2\pi-\xi_0} \frac{\cos(m\,\xi)}{\sqrt{2[\Omega - \cos\xi - \epsilon_2\,\cos(2\,\xi)]}}\,\frac{d\xi}{2\pi}, \tag{94}$$

where

$$\xi_0 = \cos^{-1}\left[\frac{-1+\sqrt{1+8\,\epsilon_2\,(\Omega+\epsilon_2)}}{4\,\epsilon_2}\right]. \tag{95}$$

Here, $0 \leq \xi_0 \leq \pi$.

It is helpful to define $p = \sqrt{(\Omega + 1 - \epsilon_2)/2}$. Thus, $p = 0$ at the magnetic O-points, and $p = 1$ at the magnetic X-points and on the magnetic separatrix. In the region $p \geq 1$, which lies outside the magnetic separatrix, let $\sin\varphi = \cos(\xi/2)$. It follows that

$$C_m(p \geq 1) = \frac{1}{\pi}\int_0^{\pi/2} \frac{\cos\left[2\,m\,\cos^{-1}(\sin\varphi)\right]}{\sqrt{p^2 - (1-4\,\epsilon_2)\,\sin^2\varphi - 4\,\epsilon_2\,\sin^4\varphi}}\,d\varphi. \quad (96)$$

In the region $0 \leq p < 1$, which lies inside the magnetic separatrix, let $\sin\varphi = \cos(\xi/2)/\cos(\xi_0/2)$. It follows that

$$C_m(0 \leq p < 1) = \frac{1}{\pi}\int_0^{\pi/2} \frac{\cos\left[2\,m\cos^{-1}(\tilde{p}\,\sin\varphi)\right]\tilde{p}\,\cos\varphi}{\sqrt{p^2 - (1-4\epsilon_2)\tilde{p}^2\,\sin^2\varphi - 4\epsilon_2\tilde{p}^4\sin^4\varphi}\,\sqrt{1-\tilde{p}^2\,\sin^2\varphi}}\,d\varphi, \quad (97)$$

where

$$\tilde{p} = \cos\left(\frac{\xi_0}{2}\right) = \left[\frac{4\,\epsilon_2 - 1 + \sqrt{(4\,\epsilon_2 - 1)^2 + 16\,\epsilon_2\,p^2}}{8\,\epsilon_2}\right]^{1/2}. \quad (98)$$

3. $\epsilon_2 > 1/4$

Suppose that $\epsilon_2 > 1/4$. In this case, for $0 \leq \xi < 2\pi$, $f(\xi)$ attains its absolute maximum value, $1 + \epsilon_2$, at $\xi = 0$, its minimum value, $-1/(8\,\epsilon_2) - \epsilon_2$, at $\xi = \cos^{-1}[-1/(4\,\epsilon_2)]$, and a local maximum value, $-1 + \epsilon_2$, at $\xi = \pi$. The topology of the magnetic field in the vicinity of the resonant surface is shown in Fig. 3. It can be seen that there is a series of heteroclinic magnetic X-points connected by a magnetic separatrix that extends over all values of ξ, and encloses a chain of magnetic islands. However, each magnetic island contains an internal magnetic separatrix that runs through an isolated magnetic X-point. The latter X-point is termed *homoclinic*. Moreover, each internal magnetic separatrix encloses two magnetic O-points straddling the internal X-point. It is clear, from a comparison of Figs. 1 and 3, that if ϵ_2 rises from a value below 1/4 to one above 1/4, then the magnetic O-points

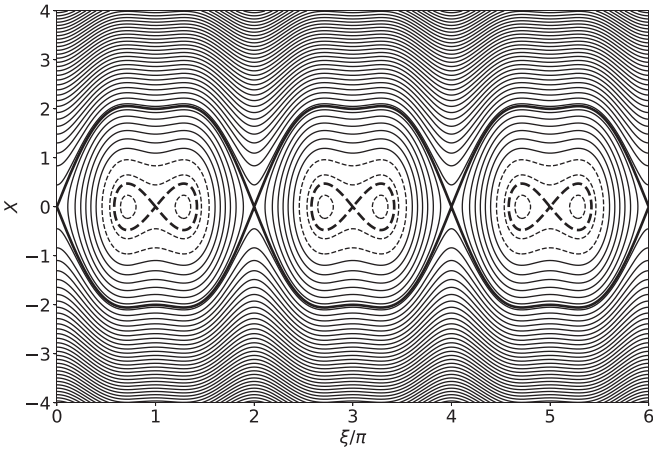

FIG. 3. Contours of the normalized magnetic flux, $\Omega(X, \xi)$, in the two-harmonic approximation for $\epsilon_2 = 0.4$. Positive/negative contours are shown as solid/dashed lines. The magnetic separatrices are shown as bold lines.

in each magnetic island shown in Fig. 1 bifurcate to give two magnetic O-points straddling a homoclinic magnetic X-point.

We can write

$$C_m(\Omega)(\Omega \geq 1 + \epsilon_2) = \int_0^{2\pi} \frac{\cos(m\,\xi)}{\sqrt{2[\Omega - \cos\xi - \epsilon_2\,\cos(2\,\xi)]}}\,\frac{d\xi}{2\pi}, \quad (99)$$

$$C_m(\Omega)(-1 + \epsilon_2 \leq \Omega < 1 + \epsilon_2) = \int_{\xi_0}^{2\pi-\xi_0} \frac{\cos(m\,\xi)}{\sqrt{2[\Omega - \cos\xi - \epsilon_2\,\cos(2\,\xi)]}}\,\frac{d\xi}{2\pi}, \quad (100)$$

and

$$C_m(\Omega)(-1/(8\,\epsilon_2) - \epsilon_2 \leq \Omega < -1 + \epsilon_2) = \int_{\xi_0}^{\xi_1} \frac{\cos(m\,\xi)}{\sqrt{2[\Omega - \cos\xi - \epsilon_2\,\cos(2\,\xi)]}}\,\frac{d\xi}{2\pi} + \int_{2\pi-\xi_1}^{2\pi-\xi_0} \frac{\cos(m\,\xi)}{\sqrt{2[\Omega - \cos\xi - \epsilon_2\,\cos(2\,\xi)]}}\,\frac{d\xi}{2\pi}, \quad (101)$$

where ξ_0 is specified in Eq. (95) and

$$\xi_1 = \cos^{-1}\left[\frac{-1 - \sqrt{1 + 8\,\epsilon_2\,(\Omega + \epsilon_2)}}{4\,\epsilon_2}\right]. \quad (102)$$

Here, $0 \leq \xi_0 \leq \xi_1 \leq \pi$.

As before, we can define $p = \sqrt{(\Omega + 1 - \epsilon_2)/2}$. Thus, $p = 0$ at the internal magnetic X-points and on the inner magnetic separatrices, and $p = 1$ at the external magnetic X-points and on the outer magnetic separatrix. In the region $p \geq 1$, which lies outside the outer magnetic separatrix, let $\sin\varphi = \cos(\xi/2)$. It follows that

$$C_m(p \geq 1) = \frac{1}{\pi}\int_0^{\pi/2} \frac{\cos\left[2\,m\,\cos^{-1}(\sin\varphi)\right]}{\sqrt{p^2 - (1-4\,\epsilon_2)\,\sin^2\varphi - 4\,\epsilon_2\,\sin^4\varphi}}\,d\varphi. \quad (103)$$

In the region $0 \leq p < 1$, which lies between the inner and outer magnetic separatrices, let $\sin\varphi = \cos(\xi/2)/\cos(\xi_0/2)$. It follows that

$$C_m(0 \leq p < 1) = \frac{1}{\pi}\int_0^{\pi/2} \frac{\cos\left[2\,m\cos^{-1}(\tilde{p}\,\sin\varphi)\right]\tilde{p}\,\cos\varphi}{\sqrt{p^2 - (1-4\epsilon_2)\tilde{p}^2\,\sin^2\varphi - 4\epsilon_2\tilde{p}^4\sin^4\varphi}\,\sqrt{1-\tilde{p}^2\,\sin^2\varphi}}\,d\varphi, \quad (104)$$

where $\tilde{p}$ is specified in Eq. (98). Let us extend the definition of p to allow it to take negative values: $p = -\sqrt{(-\Omega - 1 + \epsilon_2)/2}$. Thus, $p = 0$ on the internal magnetic separatrix, and $p = p_{\min}$, where

$$p_{\min} = -\frac{(4\,\epsilon_2 - 1)}{4\sqrt{\epsilon_2}}, \quad (105)$$

at the internal magnetic O-points. In the region, $p_{\min} \leq p < 0$, let $\sin\varphi = \cos(\xi/2)/\cos(\xi_0/2)$. It follows that

$$C_m(p_{\min} \leq p < 0) = \frac{1}{\pi}\int_{\varphi_0}^{\pi/2} \frac{\cos\left[2\,m\cos^{-1}(\tilde{p}\,\sin\varphi)\right]\tilde{p}\,\cos\varphi}{\sqrt{-p^2 - (1-4\epsilon_2)\tilde{p}^2\,\sin^2\varphi - 4\epsilon_2\tilde{p}^4\sin^4\varphi}\,\sqrt{1-\tilde{p}^2\,\sin^2\varphi}}\,d\varphi, \quad (106)$$

where

$$\varphi_0 = \sin^{-1}\left[\frac{\cos(\xi_1/2)}{\cos(\xi_0/2)}\right], \tag{107}$$

$$\tilde{p} = \cos\left(\frac{\xi_0}{2}\right) = \left[\frac{4\,\epsilon_2 - 1 + \sqrt{(4\,\epsilon_2-1)^2 - 16\,\epsilon_2\,p^2}}{8\,\epsilon_2}\right]^{1/2}, \tag{108}$$

$$\cos\left(\frac{\xi_1}{2}\right) = \left[\frac{4\,\epsilon_2 - 1 - \sqrt{(4\,\epsilon_2-1)^2 - 16\,\epsilon_2\,p^2}}{8\,\epsilon_2}\right]^{1/2}. \tag{109}$$

4. $\epsilon_2 < -1/4$

Suppose that $\epsilon_2 < -1/4$. In this case, for $0 \le \xi < 2\pi$, $f(\xi)$ attains a local minimum value, $1+\epsilon_2$, at $\xi = 0$, its maximum value, $-1/(8\,\epsilon_2) - \epsilon_2$, at $\xi = \cos^{-1}[-1/(4\,\epsilon_2)]$, and its absolute minimum value, $-1+\epsilon_2$, at $\xi = \pi$. The topology of the magnetic field in the vicinity of the resonant surface is shown in Fig. 4. It can be seen that there is a series of heteroclinic magnetic X-points connected by a magnetic separatrix that extends over all values of ξ, and encloses a chain of large magnetic islands separated by small magnetic islands. It is clear, from a comparison of Figs. 1 and 4, that if ϵ_2 falls from a value above $-1/4$ to one below $-1/4$ then each magnetic X-point shown in Fig. 1 bifurcates to give two heteroclinic magnetic X-points straddling a magnetic O-point.

We can write

$$C_m(\Omega)(\Omega \ge -1/(8\,\epsilon_2) - \epsilon_2) = \int_0^{2\pi} \frac{\cos(m\,\xi)}{\sqrt{2[\Omega - \cos\xi - \epsilon_2\,\cos(2\,\xi)]}}\frac{d\xi}{2\pi}, \tag{110}$$

$$\begin{aligned} C_m(\Omega)(1+\epsilon_2 \le \Omega < -1/(8\,\epsilon_2) - \epsilon_2) &= \int_0^{\xi_1} \frac{\cos(m\,\xi)}{\sqrt{2[\Omega - \cos\xi - \epsilon_2\,\cos(2\,\xi)]}}\frac{d\xi}{2\pi} \\ &+ \int_{\xi_0}^{2\pi-\xi_0} \frac{\cos(m\,\xi)}{\sqrt{2[\Omega - \cos\xi - \epsilon_2\,\cos(2\,\xi)]}}\frac{d\xi}{2\pi} \\ &+ \int_{2\pi-\xi_1}^{2\pi} \frac{\cos(m\,\xi)}{\sqrt{2[\Omega - \cos\xi - \epsilon_2\,\cos(2\,\xi)]}}\frac{d\xi}{2\pi}, \end{aligned} \tag{111}$$

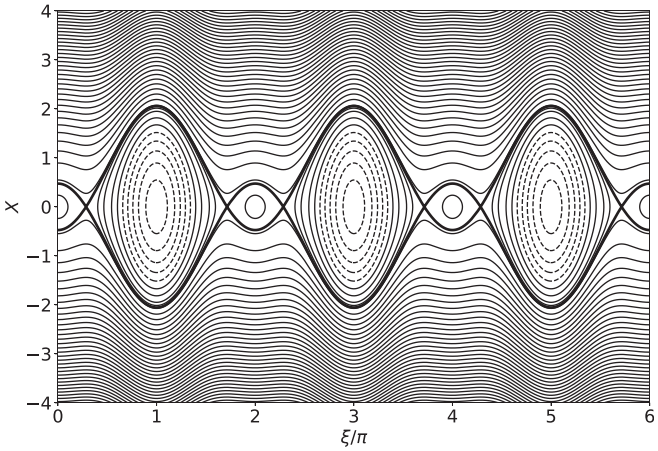

FIG. 4. Contours of the normalized magnetic flux, $\Omega(X,\xi)$, in the two-harmonic approximation for $\epsilon_2 = -0.4$. Positive/negative contours are shown as solid/dashed lines. The magnetic separatrix is shown as a bold line.

and

$$C_m(\Omega)(-1+\epsilon_2 \le \Omega < 1+\epsilon_2) = \int_{\xi_0}^{2\pi-\xi_0} \frac{\cos(m\,\xi)}{\sqrt{2[\Omega - \cos\xi - \epsilon_2\,\cos(2\,\xi)]}}\frac{d\xi}{2\pi}, \tag{112}$$

where ξ_0 and ξ_1 are specified in Eqs. (95) and (102). Here, $0 \le \xi_1 \le \xi_0 \le \pi$.

As before, we can define $p = \sqrt{(\Omega+1-\epsilon_2)/2}$. Thus, $p=0$ at the magnetic O-points of the small islands, $p=1$ at the magnetic O-points of the large islands, and $p = p_{\rm sep}$, where

$$p_{\rm sep} = \frac{1-4\,\epsilon_2}{4\sqrt{|\epsilon_2|}}, \tag{113}$$

at the magnetic X-points and on the magnetic separatrix. In the region $p > p_{\rm sep}$, which lies outside the magnetic separatrix, let $\sin\varphi = \cos(\xi/2)$. It follows that

$$C_m(p \ge p_{\rm sep}) = \frac{1}{\pi}\int_0^{\pi/2} \frac{\cos\left[2\,m\,\cos^{-1}(\sin\varphi)\right]}{\sqrt{p^2 - (1-4\,\epsilon_2)\,\sin^2\varphi - 4\,\epsilon_2\,\sin^4\varphi}}\,d\varphi. \tag{114}$$

In the region $1 \le p < p_{\rm sep}$, which lies inside both the large magnetic islands and the small magnetic islands, let $\sin\varphi = \cos(\xi/2)/\cos(\xi_0/2)$ and $\sin\varphi = \cos(\xi/2)$. It follows that

$$\begin{aligned} C_m(1 \le p < p_{\rm sep}) &= \frac{1}{\pi}\int_0^{\pi/2} \frac{\cos\left[2m\cos^{-1}(\tilde{p}\,\sin\varphi)\right]\tilde{p}\,\cos\varphi}{\sqrt{p^2-(1-4\epsilon_2)\tilde{p}^2\sin^2\varphi - 4\epsilon_2\tilde{p}^4\sin^4\varphi}\sqrt{1-\tilde{p}^2\sin^2\varphi}}\,d\varphi \\ &+ \frac{1}{\pi}\int_{\varphi_1}^{\pi/2} \frac{\cos\left[2m\cos^{-1}(\sin\varphi)\right]}{\sqrt{p^2-(1-4\epsilon_2)\sin^2\varphi - 4\epsilon_2\sin^4\varphi}}\,d\varphi, \end{aligned} \tag{115}$$

where $\tilde{p}$ is specified in Eq. (98), $\varphi_1 = \sin^{-1}[\cos(\xi_1/2)]$, and

$$\cos\left(\frac{\xi_1}{2}\right) = \left[\frac{4\,\epsilon_2 - 1 - \sqrt{(4\,\epsilon_2-1)^2 + 16\,\epsilon_2\,p^2}}{8\,\epsilon_2}\right]^{1/2}. \tag{116}$$

In the region $0 \le p < 1$, which lies inside the large magnetic islands, let $\sin\varphi = \cos(\xi/2)/\cos(\xi_0/2)$. It follows that

$$C_m(0 \le p < 1) = \frac{1}{\pi}\int_0^{\pi/2} \frac{\cos\left[2m\cos^{-1}(\tilde{p}\,\sin\varphi)\right]\tilde{p}\,\cos\varphi}{\sqrt{p^2-(1-4\epsilon_2)\tilde{p}^2\sin^2\varphi - 4\epsilon_2\tilde{p}^4\sin^4\varphi}\sqrt{1-\tilde{p}^2\sin^2\varphi}}\,d\varphi. \tag{117}$$

5. Tearing mode dispersion relation

The tearing mode dispersion relation, (69), becomes

$$\begin{pmatrix} \Delta_1' - \lambda\,I_{1,1}(\epsilon_2), & -\lambda\,I_{1,2}(\epsilon_2) \\ -\lambda\,I_{1,2}(\epsilon_2), & \Delta_2' - \lambda\,I_{2,2}(\epsilon) \end{pmatrix}\begin{pmatrix} 1 \\ \epsilon_2 \end{pmatrix} = \mu\begin{pmatrix} K_1(\epsilon_2) \\ K_2(\epsilon_2) \end{pmatrix}, \tag{118}$$

where

$$I_{m,m'}(\epsilon_2) = 8\int_{p_{\min}}^{\infty} \frac{|p|\, C_m(p)\, C_{m'}(p)}{C_0(p)}\, dp, \tag{119}$$

$$K_m(\epsilon_2) = -64\int_{p_{\min}}^{p_c} |p|\, C_m(p)\, dp, \tag{120}$$

$$p_{\min} = \begin{cases} -(4\,\epsilon_2 - 1)/\left(4\sqrt{\epsilon_2}\right) & \epsilon_2 > 1/4 \\ 0 & \epsilon_2 \leq 1/4 \end{cases}, \tag{121}$$

and

$$p_c = \begin{cases} \sqrt{(\Omega_c + 1 - \epsilon_2)/2} & \Omega_c > -1 + \epsilon_2 \\ -\sqrt{(-\Omega_c - 1 + \epsilon_2)/2} & \Omega_c \leq -1 + \epsilon_2 \end{cases}. \tag{122}$$

Equation (118) yields the quadratic equation

$$A(\epsilon_2)\,\lambda^2 + B(\epsilon_2)\,\lambda + C(\epsilon_2) = 0, \tag{123}$$

where

$$A(\epsilon_2) = I_{1,1}(\epsilon_2)\, I_{2,2}(\epsilon_2) - \left[I_{1,2}(\epsilon_2)\right]^2, \tag{124}$$

$$B(\epsilon_2) = -I_{2,2}(\epsilon_2)\,\Delta_1' - I_{1,1}(\epsilon_2)\,\Delta_2' + \mu\, I_{2,2}(\epsilon_2)\, K_1(\epsilon_2) - \mu\, I_{1,2}(\epsilon_2)\, K_2(\epsilon_2), \tag{125}$$

$$C(\epsilon_2) = \Delta_2'\left[\Delta_1' - \mu\, K_1(\epsilon_2)\right]. \tag{126}$$

Let us assume that $\Delta_1' > 0$ and $\Delta_2' < 0$. In other words, let us assume that only the $m = 1$ mode is intrinsically unstable. In this case, the most unstable root of (123) is

$$\lambda(\epsilon_2) = \frac{-B + \sqrt{B^2 - 4\,A\,C}}{2\,A}. \tag{127}$$

Here, we are assuming that $A > 0$ (as is generally the case). The dispersion relation (118) yields

$$\mathcal{F}(\epsilon_2) \equiv -\Delta_1' + \mu\, K_1(\epsilon_2) + \lambda(\epsilon_2)\, I_{1,1}(\epsilon_2) + \lambda(\epsilon_2)\,\epsilon_2\, I_{1,2}(\epsilon_2) = 0. \tag{128}$$

Thus, at fixed Δ_1', Δ_2', p_c, and μ, the determination of ϵ_2 and λ reduces to finding the root of $\mathcal{F}(\epsilon_2) = 0$.

Suppose that we increase Δ_1' while keeping the ratios Δ_2'/Δ_1' and μ/Δ_1' fixed. It is clear from the previous five equations that $\lambda \propto \Delta_1'$ and $\mathcal{F}(\epsilon_2) \propto \Delta_1'$. In other words, increasing Δ_1' in this manner leads to a proportionate increase in the growth rate of the tearing mode, and the amplitude of the non-inductive current that needs to be driven in the inner region in order to modify this growth rate but does not affect the harmonic content of the mode (i.e., the value of ϵ_2), because this content only depends on the ratios Δ_2'/Δ_1' and μ/Δ_1'.

B. Results in the absence of RF current drive

Let us first consider the nonlinear growth of the tearing mode in the absence of RF current drive. Figure 5 shows ϵ_2, which measures the ratio of the $m = 2$ to the $m = 1$ harmonics of the perturbed magnetic flux, as a function of Δ_1' for various values of Δ_2'. Note that we are assuming that $\Delta_1' \geq 0$ and $\Delta_2' \leq 0$. In other words, we are assuming that the $m = 1$ mode is intrinsically unstable, whereas the $m = 2$ mode is intrinsically stable. It can be seen that $\epsilon_2 = 0$ when $\Delta_1' = 0$. In other words, the tearing mode is exactly described by the one-harmonic approximation when it is marginally stable. However, as Δ_1' rises above zero, and the mode starts to grow, the one-harmonic approximation starts to break down. In other words, ϵ_2 becomes non-zero. It can be seen that ϵ_2 asymptotes to a finite positive value of about 0.095 in the limit that $\Delta_1' \to \infty$. Moreover, ϵ_2 attains this asymptotic value more rapidly, as Δ_1' rises, when $|\Delta_2'|$ is smaller. Note that the asymptotic value of ϵ_2 is not sufficiently positive to trigger a bifurcation of the island O-points (i.e., it is less than 1/4). Hence, we deduce that, in the absence of RF current drive, the topology of the island magnetic flux-surfaces is shown in Fig. 1.

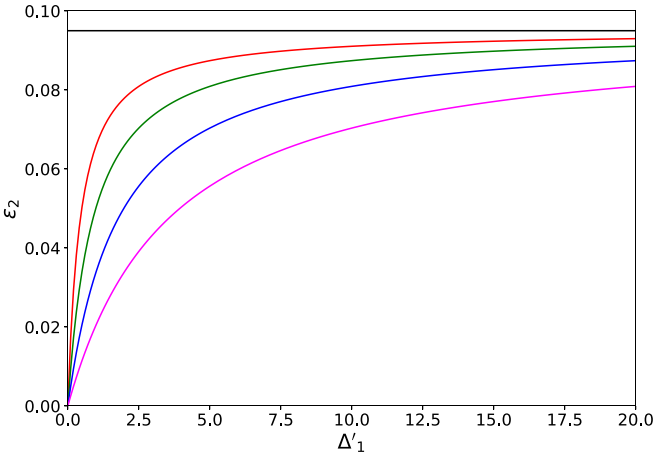

FIG. 5. ϵ_2 vs Δ_1', in the two-harmonic approximation, for a classical tearing mode in the absence of RF-driven non-inductive current. The black, red, green, blue, and magenta curves corresponds to $\Delta_2' = 0.0$, –0.5, –1.0, –2.0, and –4.0, respectively.

Figure 6 shows the difference between λ/Δ_1' in the two- and one-harmonic approximations. It can be seen that, at fixed Δ_1' and Δ_2', the normalized growth rate of the tearing mode, λ, in the two-harmonic approximation is higher than that in the one-harmonic approximation. Moreover, the relative difference asymptotes to a finite value of

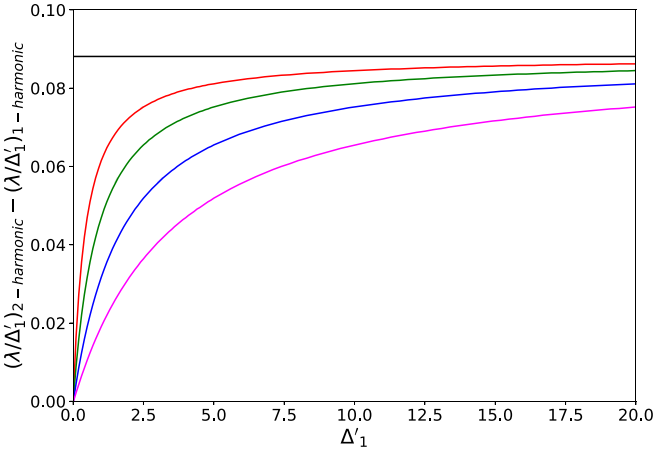

FIG. 6. Difference between λ/Δ_1' in the two- and one-harmonic approximations for a classical tearing mode in the absence of RF-driven non-inductive current. The black, red, green, blue, and magenta curves corresponds to $\Delta_2' = 0.0$, –0.5, –1.0, –2.0, and –4.0, respectively.

about 9% in the limit that $\Delta_1' \to \infty$. As before, the relative difference attains this asymptotic value more rapidly, as Δ_1' rises, when $|\Delta_2'|$ is smaller.

We conclude that, in the absence of RF current drive, the differences between the nonlinear properties of a tearing mode in the two- and one-harmonic approximations are comparatively minor.

C. Results in the presence of RF current drive

Figure 7 illustrates what happens when RF current drive is used to stabilize an intrinsically unstable tearing mode. In this particular case, $p_c = 0.2$, which implies that the current drive is strongly localized in the vicinity of the O-points of the magnetic island chain. It can be seen that, as the normalized RF current density, μ, increases, the normalized growth rate of the mode, λ, decreases. However, increasing the current density also causes ϵ_2 to increase. In fact, ϵ_2 rises above the critical value 1/4 before the mode is fully stabilized, indicating that the current drive has triggered a bifurcation of the island O-points. It can be seen that the growth rate initially decreases linearly with increasing μ, in a similar fashion to the behavior predicted in the one-harmonic approximation. However, as soon as ϵ_2 exceeds a value of about 0.1, the decrease in the growth rate with increasing μ accelerates. In fact, it is clear from the figure that the critical μ value required to stabilize the mode is significantly less in the two-harmonic approximation than in the one-harmonic approximation, indicating that the multi-harmonic content of the tearing mode (i.e., $\epsilon_2 \neq 0$) that is generated by the RF current drive facilitates the stabilization of the mode.

Figure 8 shows the critical normalized RF current density, $\mu_{\rm crit}$, needed to stabilize an intrinsically unstable tearing mode as a function of the RF injection width parameter, p_c. (For the island topology shown in Fig. 1, $p_c = 1$ corresponds to the RF-driven current filling the region inside the magnetic separatrix, and $p_c = 0$ corresponds to the current being concentrated at the island O-points. For the island topology shown in Fig. 3, $p_c = 1$ corresponds to the RF-driven current filling the region inside the outer magnetic separatrix, and $p_c = 0$ corresponds to the current filling the regions inside the inner magnetic separatrices.) Also shown is $\mu_{\rm crit}$ predicted in the one-harmonic approximation as well as the value of ϵ_2 at marginal stability. It can be seen that if the RF-driven current density is localized inside the (outer) magnetic separatrix (i.e., $p_c \lesssim 0.85$), then ϵ_2 is driven to positive values. In fact, ϵ_2 is driven to sufficiently large positive values (i.e., $\epsilon_2 > 1/4$) to trigger a bifurcation of the island O-points when $p_c \lesssim 0.25$. On the other hand, if the RF-driven current density is broadly distributed (i.e., $p_c \gtrsim 0.85$), then ϵ_2 is driven to negative values. The peak negative value of ϵ_2 occurs when $p_c \simeq 1.0$. In other words, when the RF-driven current density completely fills the region inside the (outer) magnetic separatrix. Note, however, that the peak negative value of ϵ_2 is not sufficiently negative to trigger a bifurcation of the island X-points (i.e., it is greater than $-1/4$). If the region in which the RF current is driven is much wider than the island width (i.e., $p_c \gg 1$) then $\epsilon_2 \to 0$. In other words, this case is well-described by the one-harmonic approximation. It is clear, from the figure, that the value of $\mu_{\rm crit}$ predicted in the two-harmonic approximation matches that predicted in the one-harmonic approximation as long as $|\epsilon_2| \lesssim 0.1$. On the other hand, when $p_c \lesssim 0.75$, and ϵ_2 rises above 0.1, the $\mu_{\rm crit}$ value predicted in the two-harmonic approximation is significantly less than that predicted in the one-harmonic approximation, again indicating that the multi-harmonic content of the tearing mode (i.e., $\epsilon_2 \neq 0$) that is generated by the RF current drive facilitates the stabilization of the mode.

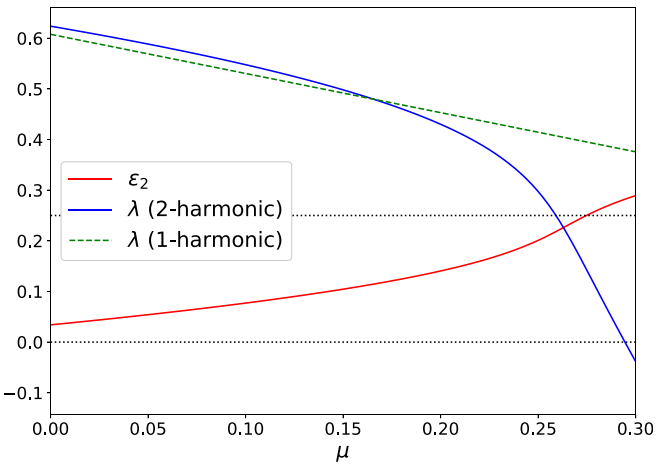

FIG. 7. Stabilization of a classical tearing mode by RF-driven non-inductive current in two- and one-harmonic approximations. The calculation is performed with $p_c = 0.2$, $\Delta_1' = 0.5$, and $\Delta_2' = -1.0$.

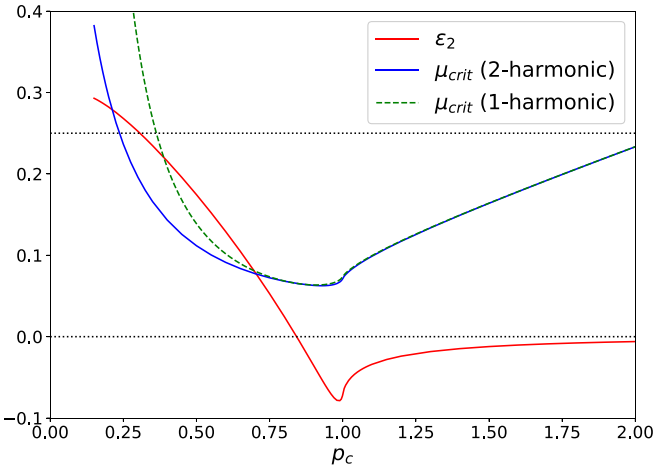

FIG. 8. Critical non-inductive RF-current drive parameter, μ, needed to stabilize a classical tearing mode, in the two- and one-harmonic approximations, as a function of the injection width parameter, p_c. The calculation is performed with $\Delta_1' = 0.5$ and $\Delta_2' = -1.0$.

We conclude that, in the presence of RF current drive, the differences between the nonlinear properties of a tearing mode in the two- and one-harmonic approximations can be significant.

VI. SUMMARY AND CONCLUSIONS

We have generalized Rutherford island theory to take into account situations in which the conventional one-harmonic approximation is not valid. Our analysis incorporates RF-driven non-inductive currents. We obtain a multi-harmonic tearing mode dispersion relation, (69), which takes the form of a nonlinear inhomogeneous matrix eigenvalue problem. The problem is nonlinear because the

matrix elements are functions of the components of the normalized eigenvector. In general, the tearing mode dispersion relation is difficult to solve because of the great multiplicity of possible magnetic flux-surface topologies in the island region. However, in the so-called two-harmonic approximation, in which we only include the principal Fourier harmonic of the perturbed magnetic flux and its first overtone in the calculation, there are only three possible flux-surface topologies. The first is the standard topology in which heteroclinic magnetic X-points alternate with magnetic O-points (see Fig. 1). The second is a topology in which each magnetic O-point undergoes a bifurcation to produce a homoclinic X-point straddled by two O-points (see Fig. 3). The third is a topology in which each magnetic X-point undergoes a bifurcation to produce two heteroclinic X-points straddling an O-point (see Fig. 4). These possibilities are sufficiently simple to allow a solution of the dispersion relation. We find that, in the absence of RF current drive, the nonlinear behavior of a tearing mode predicted in the two-harmonic approximation does not differ substantially from that predicted in the one-harmonic approximation. On the other hand, we find that RF current drive that is sufficiently localized in the vicinity of the island O-points can trigger bifurcations of the O-points (which are impossible in the one-harmonic approximation). However, the current drive does not seem capable of triggering bifurcations of the island X-points. This finding is significant because Bardóczi and Evans recently observed bifurcations of magnetic island chain O-points in the presence of RF current drive in the DIII-D tokamak[11] but did not observe bifurcations of the X-points. Finally, the changes in topology of the magnetic flux-surfaces induced by RF current drive are found to facilitate the stabilization of the mode.

In future work, we intend to generalize our analysis to cylindrical geometry, taking the bootstrap current and externally generated resonant magnetic perturbations into account. We also intend to incorporate more realistic current drive profiles into the analysis. Finally, we hope to devise a practical method of solving the full multi-harmonic dispersion relation.

ACKNOWLEDGMENTS

This research was directly funded by the U.S. Department of Energy, Office of Science, Office of Fusion Energy Sciences, under Contract Nos. DE-FG02–04ER54742 and DE-SC0021156.

AUTHOR DECLARATIONS

Conflict of Interest

The author has no conflicts to disclose.

Author Contributions

Richard Fitzpatrick: Writing – original draft (lead).

DATA AVAILABILITY

The data that support the findings of this study are available from the corresponding author upon reasonable request.

REFERENCES

[1]H. P. Furth, J. Killeen, and M. N. Rosenbluth, Phys. Fluids **6**, 459 (1963).
[2]J. A. Wesson, *Tokamaks*, 4th ed. (Oxford University Press, 2011).
[3]P. H. Rutherford, Phys. Fluids **16**, 1903 (1973).
[4]Z. Chang and J. D. Callen, Nucl. Fusion **30**, 219 (1990).
[5]R. Fitzpatrick, Phys. Plasmas **2**, 825 (1995).
[6]R. J. Bickerton, J. W. Connor, and J. B. Taylor, Nat. Phys. Sci. **229**, 110–112 (1971).
[7]R. Carrera, R. D. Hazeltine, and M. Kotschenreuther, Phys. Fluids **29**, 899 (1986).
[8]R. J. Buttery, S. Günter, G. Giruzzi, T. C. Hender, D. Howell, G. Huysmans, R. J. LaHaye, M. Maraschek, H. Reimerdes, O. Sauter, C. D. Warrick, H. R. Wilson, and H. Zohm, Plasma Phys. Controlled Fusion **42**, B61 (2000).
[9]R. J. LaHaye, Phys. Plasmas **13**, 055501 (2006).
[10]E. Westerhof, Nucl. Fusion **30**, 1143 (1990).
[11]L. Bardóczi and T. E. Evans, Phys. Rev. Lett. **126**, 085003 (2021).
[12]H. R. Strauss, Phys. Fluids **19**, 134 (1976).
[13]J. P. Freidberg, Rev. Mod. Phys. **54**, 801 (1982).
[14]C. C. Hegna and J. D. Callen, Phys. Plasmas **4**, 2940 (1997).
[15]H. Zohm, Phys. Plasmas **4**, 3433 (1997).